



Study of extrudability and standoff distance effect during nanoclay-enabled direct printing

Yifei Jin¹ · Danyang Zhao² · Yong Huang¹

Received: 17 January 2018 / Accepted: 15 March 2018 / Published online: 10 April 2018
© Zhejiang University Press 2018

Abstract

Nanoclay-enabled self-supporting printing has been emerging as a promising filament-based extrusion fabrication approach for different biomedical and engineering applications including tissue engineering. With the addition of nanoclay powders, liquid build materials may exhibit solid-like behavior upon extrusion and can be directly printed in air into complex three-dimensional structures. The objective of this study is to investigate the effect of nanoclay on the extrudability of *N*-isopropylacrylamide (NIPAAm) and the effect of standoff distance on the print quality during nanoclay-enabled direct printing. It is found that the addition of nanoclay can significantly improve the NIPAAm extrudability and effectively eliminate die swelling in material extrusion. In addition, with the increase of standoff distance, deposited filaments change from over-deposited to well-defined to stretched to broken, the filament width decreases, and the print fidelity deteriorates. A mathematical model is further proposed to determine the optimal standoff distance to achieve better print fidelity during nanoclay-enabled direct printing. Based on the extrudability and standoff distance knowledge from this study, NIPAAm–Laponite nanoclay and NIPAAm–Laponite nanoclay–graphene oxide nanocomposite hydrogel precursors are successfully printed into a three-layered one-dimensional responsive pattern, demonstrating the good extrudability and print quality during nanoclay-enabled printing under optimal printing conditions.

Keywords Extrudability · Print quality · Nanoclay · Standoff distance · Direct printing

Introduction and background

Three-dimensional (3D) bioprinting has been viewed as a promising tissue engineering solution, in particular, to on-demand fabrication of human tissues and organs [1–4]. During 3D bioprinting, human tissues and organs are fabricated layer by layer using different bioprinting approaches such as inkjet printing [5–7], laser printing [8,9], and material extrusion [10–13]. Among these fabrication approaches, material extrusion, a filament-based 3D printing approach, is widely used due to its high printing efficiency, easy implementation, and wide range of printable materials. During extrusion, the rapid solidification methodology has been widely adopted,

in which various stimuli are used to induce rapid solidification of deposited build materials in situ, such as temperature change [14,15], ultraviolet (UV) radiation [16,17], and ionic cross-linking [10,18]. However, this fabrication methodology follows the traditional “solidification-while-printing” procedure and has some constraints including the requirement of rapid solidification of liquid build materials in order to retain the printed shape and nozzle clogging. To overcome these constraints, a novel extrusion fabrication approach, nanoclay-enabled self-supporting “printing-then-solidification” [12], has been successfully demonstrated: Laponite nanoclay is used as an internal scaffold material to hold liquid 3D structures in air before solidification; after the entire 3D structure is finished, stimuli are used to cure and solidify it.

Generally, the printability during solution/suspension bioextrusion is defined as the capability of ink materials to form continuous filaments with a controllable diameter and well-defined morphology and further form 3D structures. The former is considered the extrudability, and the latter is considered the formability. Since continuous filaments

✉ Yong Huang
yongh@ufl.edu

¹ Department of Mechanical and Aerospace Engineering,
University of Florida, P. O. Box 116250, Gainesville,
FL 32611, USA

² Department of Mechanical Engineering, Dalian University of
Technology, Dalian 116023, Liaoning, China

are basic building blocks for the construction of complex 3D structures, extrudability, the formation of a controllable, continuous filament, is an important topic in the printability research. During bioextrusion, both material properties and operating conditions affect the formation of continuous filaments, which determines the precision of printed cellular constructs and location of cells in the constructs. This is particularly important in printing 3D complex heterogeneous constructs which are made of numerous deposited filaments. During conventional rapid solidification-based extrusion, the printing process has been typically investigated based on the effects of ink rheological properties and homogeneity on the printability and the evaluation of printing resolution and accuracy. For example, Chuang et al. [19] reported the filament morphology and diameter are closely dependent on the preprocessing of bioinks and their material properties during extrusion printing different sodium alginate (NaAlg)-based solutions. Kang et al. [20] printed various alginate, poly(ethylene glycol) diacrylate (PEGDA), and gelatin bioinks under different printing conditions and found that printing conditions including the nozzle diameter, dispensing pressure, path height (standoff distance), path spacing (feed), and printing speed can affect the printing accuracy and resolution of 3D structures. For nanoclay-enabled direct extrusion printing, while the effects of operating conditions on the filament diameter and morphology have been investigated during the extrusion of nanoclay-based hydrogel composite filaments [12], the influence of nanoclay on the extrudability and print quality is still to be further elucidated.

The objective of this study is to investigate the effect of nanoclay on the extrudability and the effect of standoff distance on the print quality during nanoclay-enabled direct extrusion printing. The print quality is evaluated based on the morphology (in terms of continuity and cross-sectional shape) and width of filaments as deposited as well as the print fidelity, which is defined as the variance between the design and deposited features. In this study, *N*-isopropylacrylamide (NIPAAm) is selected as a model ink material with poor extrudability. As a thermally sensitive hydrogel precursor, NIPAAm has been extensively investigated for various biological applications such as drug delivery [21,22] since its deformation can be triggered by physiological temperature conditions. To investigate the influence of nanoclay additive during nanoclay-enabled direct extrusion printing, Laponite XLG nanoclay is used as both ink material and internal scaffold material. Both Laponite and its nanocomposites have been utilized in different biomedical applications [12,23,24]. As the internal scaffold material during extrusion, Laponite XLG is added to prepare the NIPAAm–Laponite nanocomposite hydrogel precursor to investigate the improvement of the bioink extrudability. For comparison, high-concentration NaAlg, a natural polysaccharide widely used for biorelated

applications [6,7,9,10,18], is selected as a benchmark bioink material herein. In summary, four biocompatible materials (NIPAAm, Laponite, NIPAAm–Laponite, and NaAlg) are extruded through a transparent glass nozzle to study their extrudability, and the velocity field distribution is measured to evaluate the effects of nanoclay on the extrudability. The effects of standoff distance, one of the most important operating parameters, on the print quality are investigated. Furthermore, an optimal standoff distance model is established, and a one-dimensional (1D) pattern made of Laponite-based poly(*N*-isopropylacrylamide) (pNIPAAm) responsive nanocomposite hydrogel is designed and printed based on the optimal standoff distance as identified.

Materials and experimental setup

Materials

Materials for extrudability and process dynamics investigation

The NIPAAm solution (18.0% (w/v)) was prepared by dispersing the appropriate amount of dry NIPAAm (113.16 g/mole, Acros Organics, Waltham, MA) in deionized (DI) water with continuous stirring using an overhead stirrer (Thermo Fisher Scientific, Waltham, MA) at 500 rpm. The Laponite nanoclay suspension (6.0% (w/v)) was prepared by dispersing the appropriate amount of dry Laponite XLG (BYK Additives Inc., Gonzales, Texas) in DI water with continuous mixing. This was continued for a minimum of 60 min to ensure thorough hydration of Laponite, and the Laponite suspension was aged for 24 h before use. For the preparation of NIPAAm–Laponite nanocomposite hydrogel precursor suspension, 6.0% (w/v) Laponite XLG was first prepared per the above protocol. Then, the appropriate amount of NIPAAm was dispersed in the Laponite suspension at a concentration of 18.0% (w/v). The overhead stirrer was used to continuously mix the nanocomposite hydrogel precursor at 500 rpm for a minimum of 30 min. Finally, Irgacure 2959 (I-2959, Ciba, Basel, Switzerland) was added to the suspension at a concentration of 0.75% (w/v) as the ultraviolet photoinitiator and mixed thoroughly. The NaAlg solution (6.0% (w/v)) was prepared by dispersing the appropriate amount of dry NaAlg (low molecular weight (20–40 kDa), Acros Organics, Waltham, MA) in DI water with continuous stirring until complete dissolution. All materials were prepared at room temperature.

Materials for printing applications

To evaluate nanoclay as a printability enhancement additive for the direct printing of pNIPAAm-based responsive

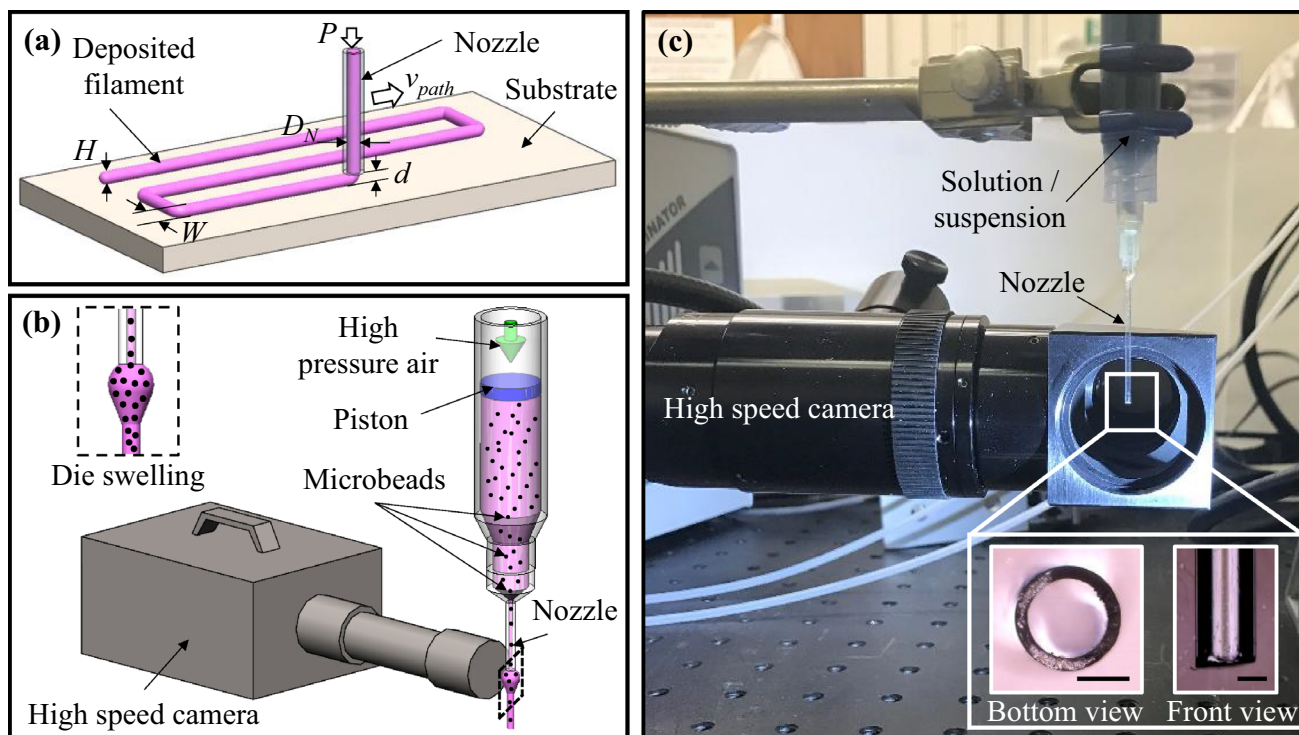


Fig. 1 **a** Schematic of material extrusion in air, **b** schematic of extrusion visualization system, and **c** experimental setup (scale bars: 500 μm)

hydrogels in air, NIPAAm–Laponite–graphene oxide (GO) nanocomposite hydrogel ink [25] was prepared in addition to the NIPAAm–Laponite nanocomposite hydrogel ink, which was prepared per the aforementioned protocol but under a continuous nitrogen flow. For the preparation of the NIPAAm–Laponite–GO nanocomposite hydrogel ink, an appropriate amount of GO (806641, Sigma-Aldrich, St. Louis, MO) was dispersed in DI water at a concentration of 0.44% (w/v). An ultrasonic vibrator (Branson 1510, Danbury, CT) was used for 60 min to disperse the GO nanoplatelets uniformly in DI water. Ice was added to the water bath of the ultrasonic vibrator every 20 min to control the bath temperature. Then Laponite nanoclay, NIPAAm, and Irgacure 2959 were added to the GO suspension sequentially under a nitrogen flow per the same protocol for the preparation of the NIPAAm–Laponite nanocomposite hydrogel ink.

Experimental setup

The filament width (W) and morphology during extrusion printing with constant pressure are significantly affected by four operating parameters including the dispensing pressure (P), nozzle path speed (v_{path}), nozzle inner diameter (D_N), and standoff distance (d) as shown in Fig. 1a in addition to ink material properties. In material extrusion, polymer-based build material fluids undergo a shear stress, resulting in stretched polymer molecular chains in the nozzle; while

at the exit of the nozzle, the disappearance of shear stress and recovery of polymer chains to a coiled state lead to the die swelling phenomenon. As such, the diameter of extrudate may be significantly larger than the nozzle inner diameter as shown in the inset of Fig. 1b. This die swelling may make it difficult to control the filament diameter.

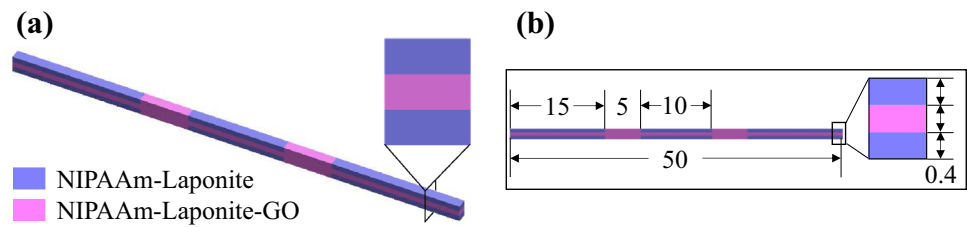
Specifically, two printing systems were set up for the proposed studies: an extrusion visualization system to investigate the effect of nanoclay on extrudability, and an extrusion fabrication system to study the standoff distance effects and the fabrication of nanocomposite hydrogel structures using nanoclay-enabled direct extrusion printing.

Extrusion visualization system for extrudability and process dynamics investigation

An extrusion visualization system as shown in Fig. 1b was designed to study the extrusion process dynamics. High pressure air was used to dispense ink materials out of a homemade glass nozzle (an inner diameter of approximately 750 μm and a length of approximately 31.75 mm as shown in the insets of Fig. 1c) to form filaments/droplets. A high-speed camera was positioned at the exit of the nozzle to image the movement of the microbeads during extrusion as illustrated in Fig. 1c.

Particle imaging velocimetry (PIV) was implemented to investigate the velocity field distribution in the extruded filament at the exit of the nozzle. Black polystyrene microbeads

Fig. 2 Design of 1D pattern for printing. **a** 3D schematic of designed 1D pattern, and **b** dimensions of the 1D pattern (unit: mm)



(6 μm diameter, Polysciences, Warrington, PA) were mixed thoroughly with NIPAAm solution, Laponite suspension, NIPAAm–Laponite suspension, and NaAlg solution at a concentration of 1.00% (v/v). These four inks mixed with the microbeads were extruded through the glass nozzle with a standoff distance of 150 mm. Based on nominal pressure conditions during printing, different pressures were utilized to extrude these four materials: 0.34×10^5 Pa (5 psi) for NIPAAm extrusion and 1.38×10^5 Pa (20 psi) for Laponite, NIPAAm–Laponite, and NaAlg extrusion. Images and videos were captured using a high-speed camera (Fastcam SA5, Photron, San Diego, CA), and the frame rate for imaging was 500 fps (frame per second). To determine the velocity field distribution in extruded droplets/filaments, a measurement plane 750 μm below the exit of the nozzle was selected and its velocity vectors along the radial direction were recorded. The data were analyzed using PIVlab (Matlab, MathWorks, Natick, MA).

Extrusion fabrication system for printing applications

The extrusion fabrication system was a microdispensing pump machine (nScript-3D-450, nScript, Orlando, FL), and all printing was conducted at ambient conditions. If not specified, a 22-gauge nozzle (410 μm inner diameter and 6.35 mm length) (EFD, Nordson, Vilters, Switzerland) was used to dispense ink materials at a path speed of 1.00 mm/s under 1.03×10^5 Pa (15 psi) (constant pressure). For the investigation of the standoff distance effects during printing, NIPAAm–Laponite filaments were printed onto a substrate when the standoff distance increased from 0.2 to 1.4 mm. For 1D pattern printing, NIPAAm–Laponite and NIPAAm–Laponite–GO filaments were printed as designed (Fig. 2a) at a standoff distance of 0.4 mm. The 1D pattern was designed with the overall length of 50.0 mm and each layer thickness of 0.4 mm as shown in Fig. 2b. After printing, an ultraviolet (UV) curing system (OmniCure Series 2000, Lumen Dynamics, Mississauga, ON, Canada) was used to cure the deposited patterns at a power of 18 W/cm^2 for 15 min. After curing, the 1D pattern was submerged in DI water at room temperature for 24 h to hydration. Then the fully swollen 1D pattern was submerged in hot water (60°C) for 5 min to deform into a two-dimensional (2D) shape.

Contact angle measurement

The cross-sectional shape of deposited filaments is affected by the standoff distance, which should be optimized based on the filament contact angle. To identify the optimal standoff distance, the contact angle of NIPAAm–Laponite nanocomposite hydrogel precursor filaments, deposited on a ceramic substrate using a dispensing nozzle (EFD, Nordson, Vilters, Switzerland) with an inner diameter of 1.50 mm, was measured using a tensiometer (Attension ThetaLite 101, Biolin Scientific, Sweden).

Effects of nanoclay on extrudability

During material extrusion, extrudability is mainly affected by the dispensing pressure and ink rheological properties. In conventional rapid solidification-based extrusion, a high dispensing pressure may lead to the formation of a jet, which may further break up into droplets in air due to the effect of surface tension and gravity, while a low dispensing pressure may cause the formation of dripping droplets especially when the ink viscosity is relatively low. For better extrudability, a suitable range of printing pressure should be identified first. Under aforementioned pressure conditions for four different inks (NIPAAm, Laponite, NIPAAm–Laponite, and NaAlg), they were extruded through the glass nozzle and the effect of the nanoclay on extrudability was investigated. Since a small amount of GO additive (0.44% (w/v)) doesn't change the rheological properties and extrudability of the NIPAAm–Laponite nanocomposite hydrogel precursor as observed, NIPAAm–Laponite–GO nanocomposite hydrogel precursor was not investigated herein.

The extrusion schematics and process images of the low-viscosity NIPAAm solution are shown in Fig. 3a-1 and a-2. Due to its low viscosity (0.002 Pa·s) and the pronounced capillary effect, the extruded NIPAAm solution cannot form a continuous filament; instead the solution forms dripping droplets after leaving the nozzle outlet. As a result, the NIPAAm solution has poor extrudability and cannot be used alone for extrusion-based printing applications. Figure 3b-1 and b-2 shows the extrusion process of the Laponite nanoclay suspension, a Bingham plastic material with the unique yield-stress property [12,13,25,26]. When extruding through

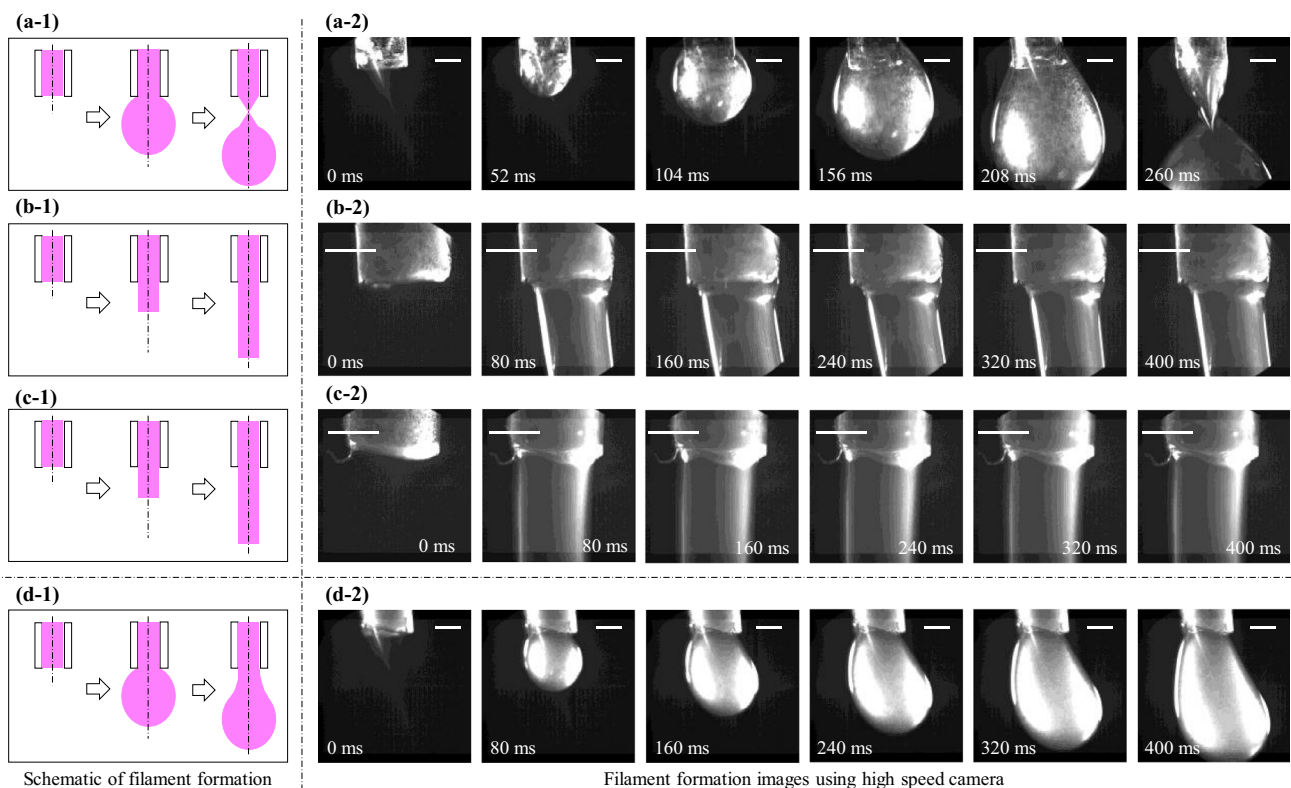


Fig. 3 Schematics and images of filament formation process of four different materials: **a** NIPAAm, **b** Laponite, NIPAAm–Laponite, and **d** NaAlg (scale bars: 500 μm)

a nozzle, the Laponite nanoclay suspension in the nozzle is sheared and behaves as a shear thinning fluid material. If the applied stress is higher than its shear yield stress, it behaves like liquid; otherwise, it behaves like solid. At the nozzle exit, the shear stress drops close to zero, resulting in a rapid liquid to solid-like transition behavior [12,25]. As a result, the extruded Laponite filament has a well-defined morphology with negligible die swelling as shown in Fig. 3b-1 and b-2. By mixing Laponite nanoclay with NIPAAm, the resulting NIPAAm–Laponite nanocomposite hydrogel precursor retains the unique yield-stress property of nanoclay suspensions and can form a filament with well-defined morphology and negligible die swelling during extrusion as shown in Fig. 3c-1 and c-2. For comparison, a high-concentration viscous NaAlg, which has a zero-shear-rate viscosity of approximately 3.1 Pa·s [27] but is not a yield-stress fluid, was extruded to examine the effect of viscosity on the extrudability. NaAlg filament formation is illustrated in Fig. 3d-1 and d-2, and though NaAlg filament does not break up into dripping droplets during extrusion due to its high viscosity, the die swelling phenomenon is pronounced. This may make it difficult to control the filament diameter, and the NaAlg filament diameter is larger than the nozzle diameter at the exit.

To further investigate the effects of the nanoclay on the extrudability, the velocity field during extrusion was measured at a plane 750 μm below the nozzle exit and analyzed using PIV, and the results are shown in Fig. 4 and Table 1. As shown in Fig. 4a, it is found that for the NIPAAm solution the diameter approximates to 2000 μm which is much larger than the nozzle inner diameter (750 μm) due to the formation of dripping droplets instead of filaments. In addition, the radial and axial velocities don't show any monotonic trend in the measurement plane, and the average radial (0.58 mm/s) and axial velocities (0.88 mm/s) are at the same scale (Table 1), indicating that a turbulent flow develops during NIPAAm droplet formation (Fig. 4a). In contrast, in Laponite nanoclay extrusion, the filament diameter (approximately 750 μm) is close to the nozzle inner diameter as shown in Fig. 4b and the radial velocity (approximately 0.06 mm/s) is negligible compared with the axial velocity (approximately 1.88 mm/s) as seen from Table 1. This demonstrates that the Laponite nanoclay suspension behaves as a laminar flow during extrusion and the die swelling is negligible. In NIPAAm–Laponite nanocomposite hydrogel precursor extrusion, a similar filament formation phenomenon can be observed: the filament diameter (approximately 750 μm) is close to the nozzle inner diameter as shown in Fig. 4c and the radial velocity (approximately 0.05 mm/s) is negligible compared with the axial

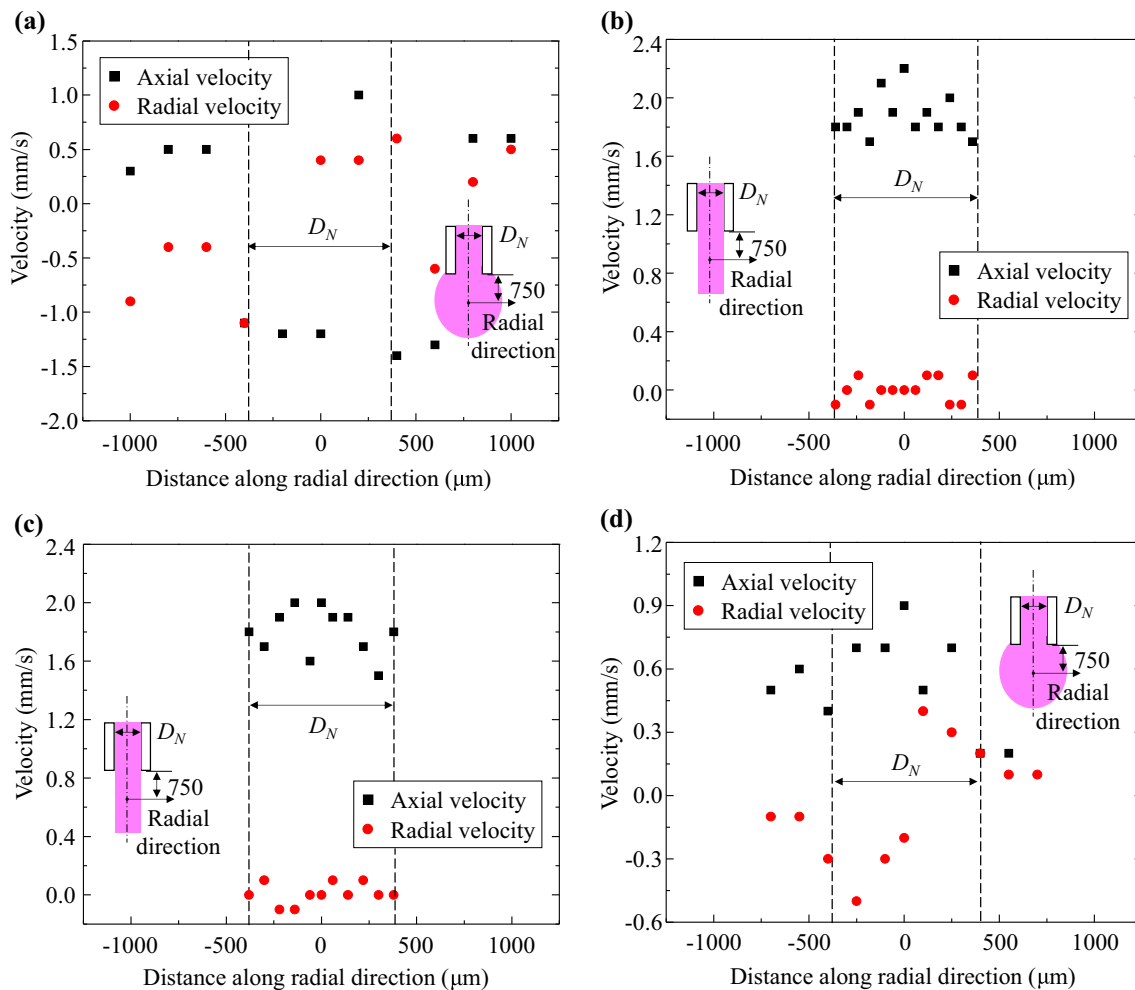


Fig. 4 PIV analysis of velocity field distribution during **a** NIPAAm, **b** Laponite, **c** NIPAAm–Laponite, and **d** NaAlg extrusion process (unit: μm)

Table 1 Velocity values along radial and axial directions

Ink material	Radial velocity (mm/s)	Axial velocity (mm/s)
NIPAAm	0.58 ± 0.27	0.88 ± 0.39
Laponite	0.06 ± 0.05	1.88 ± 0.15
NIPAAm–Laponite	0.05 ± 0.05	1.80 ± 0.01
NaAlg	0.24 ± 0.14	0.55 ± 0.22

velocity (approximately 1.80 mm/s) as shown in Table 1. It can be seen that the addition of the nanoclay can make the NIPAAm hydrogel precursor to have the yield-stress property and improve its extrudability. In NaAlg solution extrusion, NaAlg filament has a diameter (1400 μm) larger than the nozzle inner diameter, indicating that the die swelling phenomenon is pronounced as shown in Fig. 4d. The average radial (0.24 mm/s) and axial velocities (0.55 mm/s) are close to each other as seen from Table 1, and the radial velocity contributes to die swelling significantly.

In material extrusion, the ink extrudability is evaluated based on the formation of continuous filaments and controllability of the filament diameter after extrusion. The rheological properties, especially the ink viscosity or Ohnesorge number, can affect the filament formability during extrusion printing. In NIPAAm extrusion, it is difficult to form continuous filaments due to the low viscosity of the NIPAAm ink. As a rheological agent, the Laponite nanoclay can effectively increase the viscosity of ink solutions, resulting in a significant improvement of the extrudability of the NIPAAm solution. It should be noted that increasing the ink viscosity only cannot ensure the controllability of filament morphology. As seen from higher concentration NaAlg extrusion, NaAlg with higher concentration has a relatively high viscosity but the poor morphology controllability due to die swelling as seen from Fig. 4d, indicating that it is the yield-stress property that plays an important role in determining the extrudability in addition to the viscosity. When using the nanoclay as a rheological additive, the NIPAAm–Laponite nanocomposite hydrogel precursor

demonstrates the yield-stress property and can rapidly transit its state from liquid to solid-like during extrusion, which prevents filament swelling at the nozzle exit and improves the morphology controllability significantly. It should also be pointed out that polymer solution/suspension may slip over the nozzle inner surface if the shear stress exceeds a critical value, affecting the formation of continuous filaments with smooth surface [28]. During NIPAAm–Laponite extrusion, the wall slip-induced hydrodynamic instability does not show any pronounced influence as observed, and all deposited filaments have a smooth surface. As such, the addition of the nanoclay effectively improves the extrudability of NIPAAm ink solutions.

Effects of standoff distance on print quality

In conventional rapid solidification-based extrusion, the selection of standoff distance (d), the gap between nozzle tip and receiving substrate (including the surface of previously deposited layers/filaments), determines the formation of continuous filaments and successful implementation of 3D structure fabrication. If the selected standoff distance is too short, the applied solidification stimuli may cause the extruded filament to solidify in air and even in the nozzle, resulting in nozzle clogging. If the standoff distance is too long, the extruded filament may break up into dripping droplets or segments due to the effects of gravity and surface tension.

During nanoclay-enabled direct printing, since nanoclay functions as a rheological modifier with the yield-stress property to support 3D liquid structures in air, the fabrication process follows a “printing-then-solidification” style [12], in which no stimuli are applied to induce solidification until printing is finished. It is unnecessary to consider the nozzle clogging issue caused by the rapid solidification of filaments within a standoff distance. In addition, the nanoclay-induced yield-stress property of the nanocomposite hydrogel precursors prevents filament breakup which may be caused by the interfacial tension during extrusion as long as the interfacial tension is lower than the yield stress. Since the addition of nanoclay can effectively avoid the concerns of nozzle clogging and filament breakup as experienced in conventional extrusion, the selection of standoff distance during nanoclay-enabled direct printing only considers the print quality in terms of the filament morphology, filament width, and print fidelity.

Effects of standoff distance on print quality

Once a continuous filament is extruded, the print quality of filaments in terms of the filament morphology, filament width and print fidelity is influenced by the standoff distance. The

effect of standoff distance on the filament morphology is first investigated in order to examine the importance of standoff distance. As shown in Fig. 5a-1 to a-5, five types of filaments can be formed when the standoff distance increases. When the standoff distance is lower than the height of a printed filament (H), an over-deposited filament can be formed in which the filament width is extremely large and uncontrollable as shown in Fig. 5a-1. When the standoff distance is increased equivalent to the filament height, a well-defined filament without any deposition delay time ($\Delta t = \frac{d-H}{v_{\text{ink}}}$, where v_{ink} is the velocity of extruded nanocomposite hydrogel precursors at the nozzle exit) can be formed. The deposition delay time is defined as the time required for an extruded filament to travel through air before landing on a receiving substrate. The morphology of deposited filaments is well-shaped, and the filament width is predictable and controllable as shown in Fig. 5a-2. When the standoff distance is a little higher than the filament height, the nanocomposite hydrogel precursor filament turns solid-like during deposition due to its yield-stress property, so the gravity and dragging effect on the printed filament can be neglected. As such, the deposited filament is still well-defined, and the filament width is close to that of the well-defined filament printed under the aforementioned standoff distance condition (zero deposition delay time). Since there is a gap between the nozzle tip and deposited filament, the deposition delay time may influence the deposition process. Such a filament is designated as a well-defined filament with a deposition delay time as shown in Fig. 5a-3. When the standoff distance further increases, the gravity and dragging effects become more significant, resulting in a stretched filament whose width decreases dramatically as shown in Fig. 5a-4 and finally breaks into droplets (broken filament) as shown in Fig. 5a-5 if the standoff distance keeps increasing.

Furthermore, the effect of standoff distance on the filament width is studied as illustrated in Fig. 5b. As shown in Fig. 5b, when the standoff distance is relatively small (for example, 0.2 mm), an over-deposited filament is formed, and the filament width is extremely large. With an increasing standoff distance, the filament width decreases significantly. When the standoff distance increases from 0.4 to 0.6 mm, the variance of filament width is negligible, indicating that the optimal standoff distance to form well-defined filaments without deposition delay time is approximately 0.4 mm. When the standoff distance increases further, the filament width decreases again, and the stretched filament forms. Finally, the broken filament forms on the receiving substrate if the standoff distance increases higher than 1.4 mm in this study.

The effect of standoff distance on the print fidelity is also investigated in terms of how a deposited pattern follows the designed printing path as shown in Fig. 5c. When the standoff distance is smaller than or equal to the height

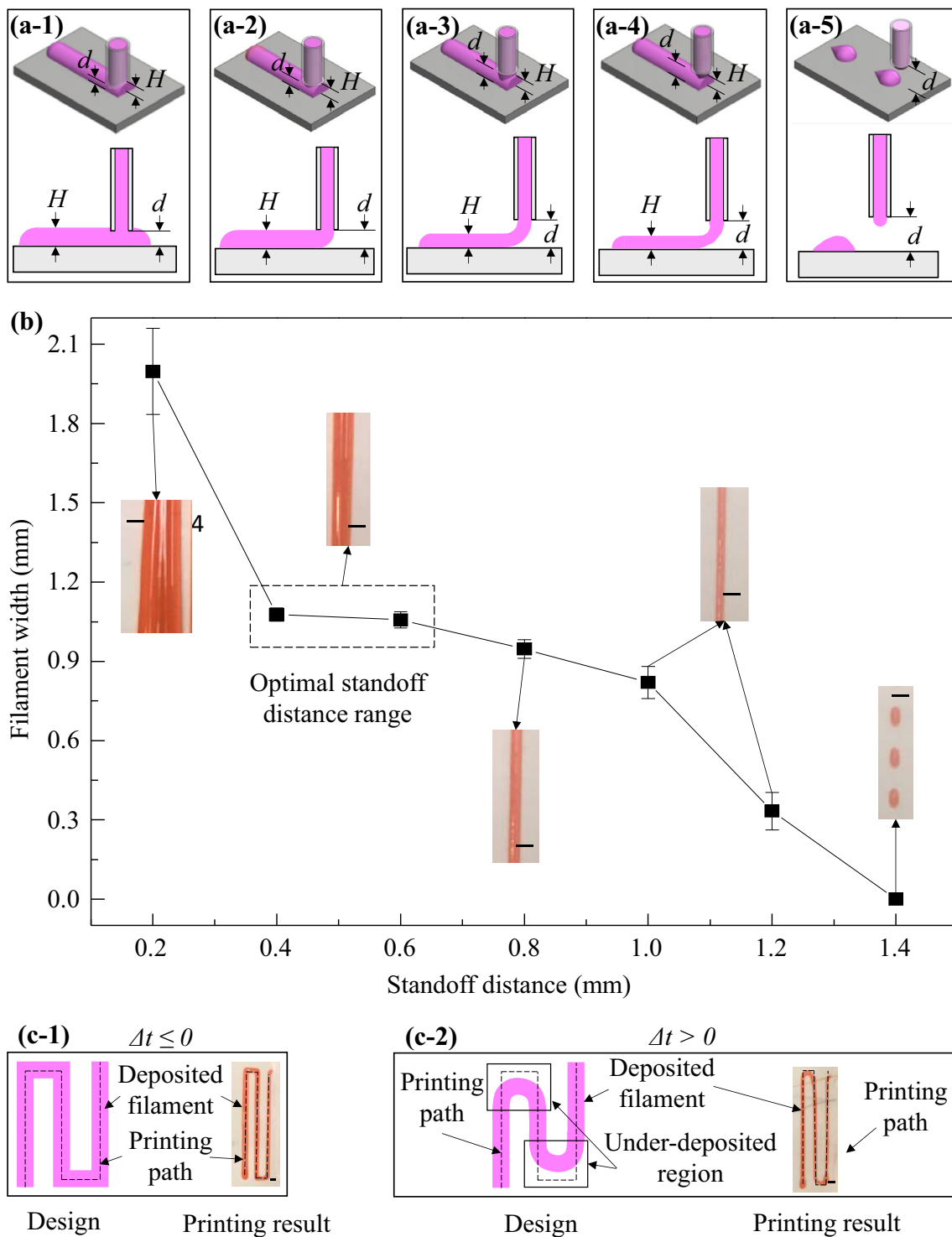


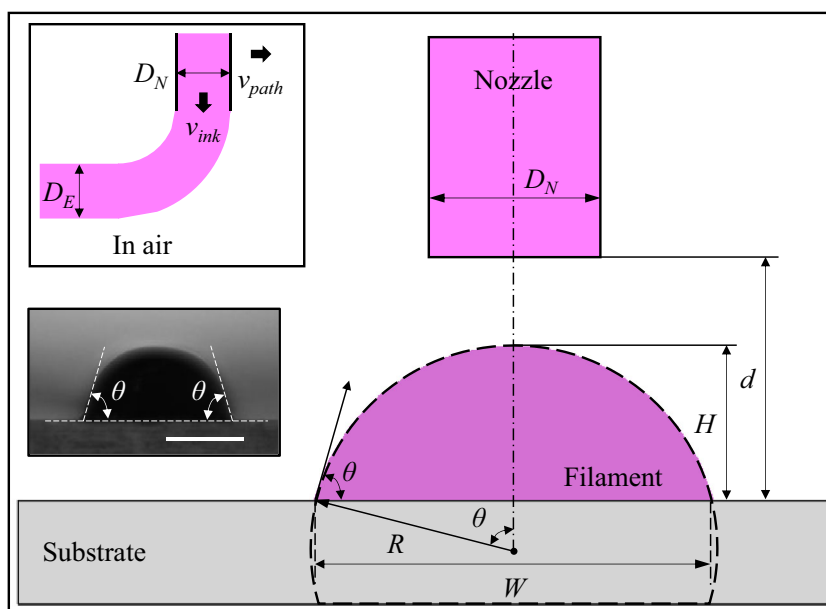
Fig. 5 Effects of standoff distance on the print quality. **a** Effect of standoff distance on the filament morphology: **a-1** over-deposited filament, well-defined filament **a-2** without deposition delay time and **a-3** with

deposition delay time, **a-4** stretched filament, and **a-5** broken filament, **b** effect of standoff distance on the filament width, and **c** effect of standoff distance on the print fidelity (scale bars: 1.0 mm)

of printed filaments, there is no gap between the nozzle tip and deposited filament, and the deposition delay time is negligible. As a result, the filament can be deposited exactly

along the designed printing path (marked using the dashed lines) as shown in Fig. 5c-1. When the standoff distance increases larger than the filament height, there is a deposition

Fig. 6 Schematics of filament deposition on substrate



delay time, which leads to the under-deposition phenomenon; especially around deposition corners, the extruded filament (shaded) may not be deposited exactly according to the designed printing path as shown in Fig. 5c-2 due to the effect of the deposition delay time that is determined by the gap between the nozzle tip and receiving substrate.

Estimation of optimal standoff distance

The filament formation and deposition process on a substrate can be divided into two sequential processes: filament extrusion in air and filament deposition on the substrate. During filament deposition, the print quality is largely affected by the standoff distance as seen from Fig. 5, and the optimal standoff distance is studied based on the following four assumptions: (1) during extrusion the cross-sectional area of a filament is constant, (2) the diameter change of an extruded filament in air is only affected by v_{ink} and v_{path} , (3) the cross-sectional shape change of a filament dose not influence the filament length, and (4) the surface tension effect has a shorter time scale compared with that of the liquid to solid-like thixotropic transition during filament formation and deposition and the formation of contact angle upon deposition is not affected by the physical cross-linking process of nanoclay suspension.

As reported in a previous study [26], v_{path} can affect the filament diameter significantly during material extrusion. The effect of v_{path} on the filament diameter is pronounced during filament extrusion when a filament is first extruded out of the nozzle with an initial diameter equivalent to D_N and a speed of v_{ink} , which is a function of the pressure, path speed, nozzle geometries, and rheological properties as reported [26]. Then the extruded filament moves at a speed equivalent to v_{path} with an equivalent filament diameter (D_E). Based on

the constant volume of extruded materials, D_E can be determined as follows:

$$Q = \frac{1}{4} \pi D_N^2 v_{ink} = \frac{1}{4} \pi D_E^2 v_{path} \tag{1}$$

$$D_E = \sqrt{\frac{v_{ink}}{v_{path}}} D_N \tag{2}$$

where Q is the flow rate.

During filament deposition, the filament cross-sectional shape changes from circular to cambered as shown in Fig. 6 due to the gravity and surface tension. The radius (R) of the cambered shape can be determined based on the constant cross-sectional area as follows:

$$\frac{1}{4} \pi D_E^2 = \frac{2\theta}{360^\circ} \pi R^2 - R^2 \sin \theta \cos \theta \tag{3}$$

$$R = \sqrt{\frac{\pi}{4\theta - 2 \sin 2\theta}} D_E \tag{4}$$

where θ is the contact angle between the filament (Laponite nanoclay-based nanocomposite hydrogel precursor filament herein) and substrate. Since R can also be calculated by Eq. (5):

$$R = \frac{H}{1 - \cos \theta} \tag{5}$$

H is then estimated as follows:

$$H = \frac{(1 - \cos \theta) \sqrt{\pi}}{\sqrt{4\theta - 2 \sin 2\theta}} D_E \tag{6}$$

Equation (6) could be further simplified as $H = C D_E$, where C ($C = \frac{(1 - \cos \theta) \sqrt{\pi}}{\sqrt{4\theta - 2 \sin 2\theta}}$) is a constant as a function of contact

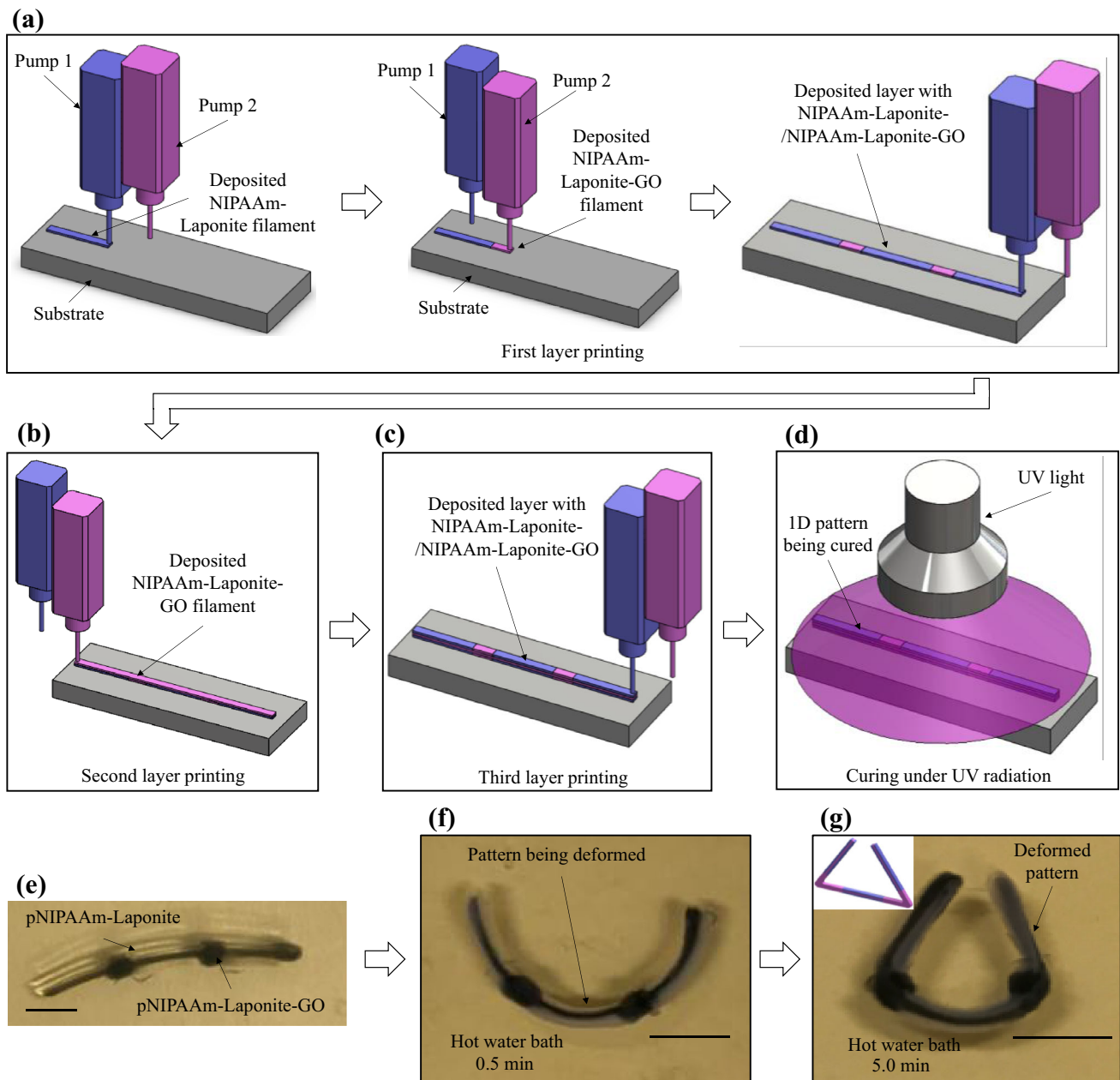


Fig. 7 Pattern printing and deformation. **a** First layer, **b** second layer, and **c** third layer printing using optimal standoff distance, **d** UV curing of printed three-layered 1D pattern, **e** cured 1D pattern swelling in DI

water bath at room temperature, and **f**, **g** gradually deforming in a hot water bath (unit: mm and scale bars: 10.0 mm)

angle. When the deposition delay time equals 0, the deposited filament may follow the designed printing path exactly. As such, the theoretical optimal standoff distance is determined as $d = C \sqrt{\frac{v_{\text{ink}}}{v_{\text{path}}}} D_N$.

The contact angle of the NIPAAm–Laponite nanocomposite hydrogel precursor is measured as shown in the inset of Fig. 6, and the average value is approximately 75.5° , resulting in a *Cof* of 0.64. Generally, v_{ink} can be estimated by $v_{\text{ink}} = \frac{P}{8\eta_0 L} R_N^2$ [26], where η_0 is the zero-shear-rate viscosity

of ink materials, L is the nozzle length, and R_N is the nozzle radius. Considering the geometries of both homemade nozzle used in the extrudability investigation and dispensing nozzle used in the standoff distance investigation, v_{ink} herein can be approximated as 2.13 mm/s based on the measured axial velocity (1.8 mm/s) during the extrudability investigation. Since v_{path} is selected as 1.00 mm/s, D_E is estimated as 598.38 μm (Eq. (2)) and the theoretical optimal standoff distance is further determined as 383.37 μm , matching the

optimal standoff distance range (Fig. 5b) as observed experimentally.

Nanocomposite hydrogel direct printing application

The extrudability and standoff distance investigation provides a practical guide for nanocomposite hydrogel printing applications. Using the identified optimal printing conditions (standoff distance: 0.4 mm, dispensing pressure: 1.03×10^5 Pa (15 psi), and path speed: 1.00 mm/s), a nanocomposite hydrogel structure was fabricated based on the design as shown in Fig. 2.

Recently, responsive material printing has emerged as a promising method to print simple patterns/structures first and then deform into complex structures upon different stimuli. Such responsive material-based fabrication strategy is widely adopted for biomedical applications such as drug delivery systems [21,22,29,30] and artificial muscles [31], to name a few. In this study two nanoclay-enabled responsive materials (NIPAAm–Laponite and NIPAAm–Laponite–GO precursors [25]) were printed to fabricate a three-layered 1D pattern (Fig. 2) directly in air. After printing, the 1D pattern was UV cured and hydrated in DI water at room temperature. To induce deformation, the hydrated 1D pattern was submerged in hot water. When the ambient temperature is higher than the lower critical solution temperature (LCST, approximately 33 °C) of the pNIPAAm-based nanocomposite hydrogels, the pNIPAAm component of the nanocomposite hydrogels changes from hydrophilic to hydrophobic and releases water molecules from the polymeric matrix, resulting in shrinking of the nanocomposite hydrogels. Due to the shrinking ratio difference between the pNIPAAm–Laponite and pNIPAAm–Laponite–GO layers, an interfacial stress develops between adjacent layers, leading to the deformation of the printed 1D pattern to a 2D shape.

In this study, the design of the 1D pattern was based on a previous study [32]. During printing, two independent dispensing pumps (Pumps 1 and 2) were utilized to sequentially deposit corresponding Laponite nanoclay-based NIPAAm nanocomposite hydrogel precursors to form the first layer as shown in Fig. 7a based on the identified optimal standoff distance. Then, Pump 2 was used to deposit the NIPAAm–Laponite–GO filament to form the second layer atop the previous ungelled layer as shown in Fig. 7b. Finally, the third layer was deposited as shown in Fig. 7c per the same protocol for the first layer printing to fabricate the three-layered 1D pattern. After printing, the 1D pattern was exposed to UV radiation for curing as shown in Fig. 7d. After curing, the solidified pattern was submerged in DI water for hydration as shown in Fig. 7e. Then the hydrated 1D pattern was submerged in a 60 °C hot water bath to induce the deformation

from a line to a triangle at 0.5 and 5.0 min as shown in Fig. 7f and g, which is similar to that as reported in a previous study [32]. This three-layered 1D pattern printing and deformation case demonstrates the good extrudability and print quality during nanoclay-enabled printing under optimal printing conditions, which may facilitate more nanoclay-based printing applications.

Conclusions and future work

This study has investigated the effect of nanoclay on the extrudability of NIPAAm and the effects of standoff distance on the printing quality during nanoclay-enabled direct printing, and main conclusions are listed as follows:

1. With the addition of Laponite nanoclay as a rheological modifier, the NIPAAm extrudability can be significantly improved and die swelling phenomenon can be effectively eliminated during extrusion printing;
2. Standoff distance during nanoclay-enabled direct printing can affect the print quality significantly. With the increase of standoff distance, the filament morphology changes from over-deposited to well-defined (without and with deposition delay time) to stretched and finally to broken, and the filament width decreases;
3. Standoff distance can also affect the print fidelity significantly. When the standoff distance is lower than or close to the height of a deposited filament, the print fidelity is satisfactory; otherwise, there is a deposition delay time which deteriorates the print fidelity during nanoclay-enabled direct printing; and
4. An optimal standoff distance model is proposed, which can be used to guide the selection of standoff distance for better printing performance. The extrudability and standoff distance knowledge herein can facilitate printing applications as witnessed during pNIPAAm–Laponite and pNIPAAm–Laponite–GO nanocomposite hydrogel pattern printing.

Future work may focus on the construction of comprehensive phase diagrams to understand the filament formation mechanisms in both conventional and nanoclay-enabled self-supporting extrusion printing approaches and further predict the formation of different filament types. In addition, future work may include improvement of the proposed standoff distance model by considering other factors such as gravity and ink rheological properties.

Acknowledgements This study was partially supported by the U.S. National Science Foundation (NSF CMMI-1634755).

References

- Mironov V, Visconti RP, Kasyanov V, Forgacs G, Drake CJ, Markwald RR (2009) Organ printing: tissue spheroids as building blocks. *Biomaterials* 30(12):2164–2174
- Ringeisen BR, Pirlo RK, Wu PK, Boland T, Huang Y, Sun W, Chrisey DB (2013) Cell and organ printing turns 15: diverse research to commercial transitions. *MRS Bull* 38(10):834–843
- Murphy SV, Atala A (2014) 3D bioprinting of tissues and organs. *Nat Biotechnol* 32(8):773–785
- Huang Y, Leu MC, Mazumder J, Donmez A (2015) Additive manufacturing: current state, future potential, gaps and needs, and recommendations. *ASME J Manuf Sci Eng* 137(1):014001-1-10
- Roth EA, Xu T, Das M, Gregory C, Hickman JJ, Boland T (2004) Inkjet printing for high-throughput cell patterning. *Biomaterials* 25(17):3707–3715
- Xu C, Chai W, Huang Y, Markwald RR (2012) Scaffold-free inkjet printing of three-dimensional zigzag cellular tubes. *Biotechnol Bioeng* 109(12):3152–3160
- Christensen K, Xu C, Chai W, Zhang Z, Fu J, Huang Y (2015) Freeform inkjet printing of cellular structures with bifurcations. *Biotechnol Bioeng* 112(5):1047–1055
- Barron JA, Ringeisen BR, Kim H, Spargo BJ, Chrisey DB (2004) Application of laser printing to mammalian cells. *Thin Solid Films* 453:383–387
- Xiong R, Zhang Z, Chai W, Huang Y, Chrisey DB (2015) Freeform drop-on-demand laser printing of 3D alginate and cellular constructs. *Biofabrication* 7(4):045011-1-13
- Khalil S, Sun W (2007) Biopolymer deposition for freeform fabrication of hydrogel tissue constructs. *Mater Sci Eng C* 27(3):469–478
- Jin Y, Compaan AM, Bhattacharjee T, Huang Y (2016) Granular gel support-enabled extrusion of three-dimensional alginate and cellular structures. *Biofabrication* 8(2):025016-1-12
- Jin Y, Liu C, Chai W, Compaan AM, Huang Y (2017) Self-supporting nanoclay as internal scaffold material for direct printing of soft hydrogel composite structures in air. *ACS Appl Mater Interfaces* 9(20):17456–17465
- Jin Y, Compaan AM, Chai W, Huang Y (2017) Functional nanoclay suspension for printing-then-solidification of liquid materials. *ACS Appl Mater Interfaces* 9(23):20057–20066
- Landers R, Hübner U, Schmelzeisen R, Mülhaupt R (2002) Rapid prototyping of scaffolds derived from thermoreversible hydrogels and tailored for applications in tissue engineering. *Biomaterials* 23(23):4437–4447
- Fedorovich NE, De Wijn JR, Verbout AJ, Alblas J, Dhert WJ (2008) Three-dimensional fiber deposition of cell-laden, viable, patterned constructs for bone tissue printing. *Tissue Eng Part A* 14(1):127–133
- Hockaday LA, Kang KH, Colangelo NW, Cheung PYC, Duan B, Malone E, Wu J, Girardi LN, Bonassar LJ, Lipson H, Chu CC, Butcher JT (2012) Rapid 3D printing of anatomically accurate and mechanically heterogeneous aortic valve hydrogel scaffolds. *Biofabrication* 4(3):035005
- Bertassoni LE, Cardoso JC, Manoharan V, Cristino AL, Bhise NS, Araujo WA, Zorlutuna P, Vrana NE, Ghaemmaghami AM, Dokmeci MR, Khademhosseini A (2014) Direct-write bioprinting of cell-laden methacrylated gelatin hydrogels. *Biofabrication* 6(2):024105
- Ozolat IT, Hospodiuk M (2016) Current advances and future perspectives in extrusion-based bioprinting. *Biomaterials* 76:321–343
- Chung JH, Naficy S, Yue Z, Kapsa R, Quigley A, Moulton SE, Wallace GG (2013) Bio-ink properties and printability for extrusion printing living cells. *Biomater Sci* 1(7):763–773
- Kang KH, Hockaday LA, Butcher JT (2013) Quantitative optimization of solid freeform deposition of aqueous hydrogels. *Biofabrication* 5(3):035001
- Schmaljohann D (2006) Thermo- and pH-responsive polymers in drug delivery. *Adv Drug Deliv Rev* 58(15):1655–1670
- Wei H, Zhang X, Cheng C, Cheng SX, Zhuo RX (2007) Self-assembled, thermosensitive micelles of a star block copolymer based on PMMA and PNIPAAm for controlled drug delivery. *Biomaterials* 28(1):99–107
- Gaharwar AK, Peppas NA, Khademhosseini A (2014) Nanocomposite hydrogels for biomedical applications. *Biotechnol Bioeng* 111(3):441–453
- Xavier JR, Thakur T, Desai P, Jaiswal MK, Sears N, Cosgriff-Hernandez E, Gaharwar AK (2015) Bioactive nanoengineered hydrogels for bone tissue engineering: a growth-factor-free approach. *ACS Nano* 9(3):3109–3118
- Jin Y, Shen Y, Yin J, Qian J, Huang Y (2018) Nanoclay-based self-supporting responsive nanocomposite hydrogels for printing applications. *ACS Appl Mater Interfaces* 10(12):10461–10470
- Jin Y, Chai W, Huang Y (2017) Printability study of hydrogel solution extrusion in nanoclay yield-stress bath during printing-then-gelation biofabrication. *Mater Sci Eng C* 80:313–325
- Zhang Z, Xiong R, Mei R, Huang Y, Chrisey DB (2015) Time-resolved imaging study of jetting dynamics during laser printing of viscoelastic alginate solutions. *Langmuir* 31(23):6447–6456
- Piau JM, El Kissi N, Tremblay B (1990) Influence of upstream instabilities and wall slip on melt fracture and sharkskin phenomena during silicones extrusion through orifice dies. *J Non Newton Fluid Mech* 34(2):145–180
- Liu L, Wang W, Ju XJ, Xie R, Chu LY (2010) Smart thermo-triggered squirting capsules for nanoparticle delivery. *Soft Matter* 6(16):3759–3763
- Yan B, Boyer JC, Habault D, Branda NR, Zhao Y (2012) Near infrared light triggered release of biomacromolecules from hydrogels loaded with upconversion nanoparticles. *J Am Chem Soc* 134(40):16558–16561
- Feinberg AW, Feigel A, Shevkoplyas SS, Sheehy S, Whitesides GM, Parker KK (2007) Muscular thin films for building actuators and powering devices. *Science* 317(5843):1366–1370
- Peng X, Li Y, Zhang Q, Shang C, Bai QW, Wang H (2016) Tough hydrogels with programmable and complex shape deformations by ion dip-dyeing and transfer printing. *Adv Funct Mater* 26(25):4491–4500